Tunable Interlayer Interactions in 2D van der Waals Frameworks

Jacob McKenzie,[a] Doran L. Pennington[a], Kentaro Kadota[a], Thomas Ericson[b], Elana Cope,[a]
Anthony F. Cozzolino,[b] Christopher H. Hendon,[a]* Carl K. Brozek [a]*
[a]*Department of Chemistry and Biochemistry, Materials Science Institute,*
University of Oregon, Eugene, OR 97403
[b]*Department of Chemistry and Biochemistry, Texas Tech University, Lubbock, TX, 79409*

Abstract. Two-dimensional materials can be isolated as monolayer sheets when interlayer interactions involve weak van der Waals forces. These rigorously atomically thin structures enable novel topological physics and open chemical questions of how to tune the structure and properties of the sheets while maintaining the sheets as isolated monolayers. Interactions between sheets and the properties they generate remain relatively neglected, as a consequence of this focus on their properties as monolayers. Here, we investigate two-dimensional porous sheets that exfoliate into isolated monolayers, but aggregate upon oxidation, giving rise to tunable interlayer charge transfer absorption and Stokes-shifted photoluminescence. This optical behavior resembles interlayer excitons, now intensely studied due to their long-lived emission, but which remain difficult to tune through synthetic chemistry. Instead, the interlayer excitons of these framework sheets can be modulated through control of solvent, electrolyte, oxidation state, and the composition of the framework building blocks. In comparison to other two-dimensional materials, these framework sheets display the largest known interlayer binding strengths, attributable to interactions between specific components within the sheets. Taken together, these results provide a microscopic basis for manipulating long-range opto-electronic behavior in van der Waals materials through molecular synthetic chemistry.

Introduction

Graphene, CrI_3, and other layered compounds derive their unique properties from weak interlayer van der Waals interactions that allow them to exist as atomically thin sheets. These 2D van der Waals (vdW) materials display distinct quantum mechanical behavior that finds use in a range of technologies including batteries,[1,2] catalysts,[3,4] superconductors,[5,6] topological insulators,[7] and photovoltaic devices.[8] However, strong interlayer interactions can also dominate the behavior of 2D vdW materials. For example, whereas monolayers of black phosphorous possess an optical band gap of 1.55 eV, the gap decreases to 1.05 eV for dimers and just 0.46 eV for bulk.[9] In addition, the already-high charge mobility of 286 $cm^2\ V^{-1}\ s^{-1}$ of black phosphorous when prepared as several stacked layers increases to 1000 $cm^2\ V^{-1}\ s^{-1}$ simply by increasing the film thickness.[10] Similar layer-dependent phenomena manifest in telurene (2D elemental Te) and certain metal chalcogenides including InSe, TiS_2, SnS, and the group-10 family (e.g., PtS_2 or $PtTe_2$).[11–16] On the other hand, various classes of layered materials, including the group-6 and group-7 transition metal dichalcogenides (e.g., WSe_2 and MoS_2) and ReS_2, display little if any dependence on layer thickness.[16] This marked difference in interlayer interactions has been correlated with interlayer binding strengths, which range from 23 meV $Å^{-2}$ for weakly interacting graphene to 33 meV $Å^{-2}$ for strongly interacting black phosphorous.[17] Microscopically, "quasi-covalent bonding" between electron lone pairs in the so-called van der Waals gap between these layered compounds has been postulated as the origin of strong interlayer interactions. In fact, X-ray scattering measurements

https://doi.org/10.26434/chemrxiv-2024-n5dl2 ORCID: https://orcid.org/0000-0002-8014-7904 Content not peer-reviewed by ChemRxiv. License: CC BY-NC-ND 4.0

have detected electron density between TiS_2 sheets resembling S-S bonding interactions.[18] Beyond single-compound materials, interlayer interactions influence heterostructures as well. Practically, exciton annihilation rates in MoS_2 and WS_2 can be reduced by 1 to 2 orders of magnitude by using a Al_2O_3 or $SrTiO_3$ substrate as opposed to a quartz substrate.[19] Furthermore, band-edge offsets in heterojunctions such as $MoSe_2/WSe_2$ lead to interlayer excitons[20] with long recombination lifetimes and ultra-high charge carrier/thermal transport due to efficient polaron delocalization across layers[21,22] Interlayer excitons find utility in advanced field-effect transistors,[23,24] photodetectors,[25,26] and quantum emitters.[27] Despite the importance of interlayer interactions in tuning 2D vdW behavior, little is known about their chemistry, in part due to the limited set of materials and synthetic methods for investigating them.

Here, we report a combined experimental-computational investigation into the tunable interlayer interactions of the 2D metal-organic framework (MOF) $Fe(SCN)_2(pyrazine)_2$. These 2D materials exfoliate under sonication to yield a colorless solution of colloidally stable monolayer sheets with Fe in the 2+ oxidation state, but upon either chemical or electrochemical oxidation, an intense and broad absorption band is introduced. DFT calculations indicate that oxidation creates mixtures of Fe^{3+}/Fe^{2+} sheets that strongly interact with an anomalously large binding strength of ca. 64 meV/Å^2. Simulations also suggest that this absorption band arises from interlayer charge transfer from the S atom of an Fe^{3+}-SCN fragment in one layer to a pyrazine ring in the next layer through the vdW gap. Although this excitation resembles interlayer excitons, it occurs between materials that differ only in oxidation state rather than between heterodimers. Whereas interlayer excitons and binding strengths remain difficult to tune in conventional vdW materials,[28] the 2D vdW MOF is amenable to a range of chemical modification strategies. Experimentally, this interlayer charge transfer can be modulated with solvents of varying dielectric strength to screen the interlayer interaction, with electrolyte to separate the sheets, or by altering the chemical composition of the donor-acceptor components of the 2D MOF. Taken together, these results expand the types of interlayer interactions through synthetic tunability, while inching their orbital nature closer towards true covalent binding.

Results and Discussion

In search of vdW materials with wide synthetic tunability, we targeted a subset of MOF structures due to their diverse compositions. Although most MOFs are electronic insulators, a growing family of atomically thin structures show the semiconducting or metallic behavior expected for vdW materials with strong interlayer interactions.[29] Indeed, recent reports indicate that charge mobility between sheets may exceed mobility within a 2D sheet.[30] However, studies of interlayer interactions between 2D MOFs remains largely limited to the "graphitic", honeycomb-type structures dominated primarily by π–π forces akin to graphene.[31] Inspired by the ability of the lone pairs in black phosphorous or TiS_2 to interact across the vdW gap, we targeted the 2D layered MOF $Fe(SCN)_2(pyz)_2$ (Fe-SCN-pyz, **Fig. 1a, 1c**), which features axial SCN^- groups. We hypothesized that in a similar manner to lone pairs, the SCN^- groups would mediate vdW interactions and increase the accessible contact area between sheets. Similar pyrazine-bridged materials have exhibited semiconductor behavior.[32] Fe-SCN-pyz was prepared according to reported synthetic procedures[33] and the obtained microcrystalline powder was analyzed by powder X-ray diffraction (PXRD), which showed the expected Bragg reflections for a layered structure (**Fig. 1d**). To generate isolated 2D sheets, the bright orange microcrystalline powder was exfoliated via ultrasonication in methanol to yield an optically clear yellow solution, which strongly

https://doi.org/10.26434/chemrxiv-2024-n5dl2 **ORCID:** https://orcid.org/0000-0002-8014-7904 Content not peer-reviewed by ChemRxiv. **License:** CC BY-NC-ND 4.0

displayed the Tyndall effect (**Fig. 1b**). In addition to methanol, the material was readily suspended within a variety of both polar and nonpolar solvents (**Fig. S4**). To confirm sample stability, this nanosheet suspension was dried to yield a light orange powder and analyzed again by PXRD, confirming retention of crystallinity, with strong preferential orientation along the (001) crystallographic plane.

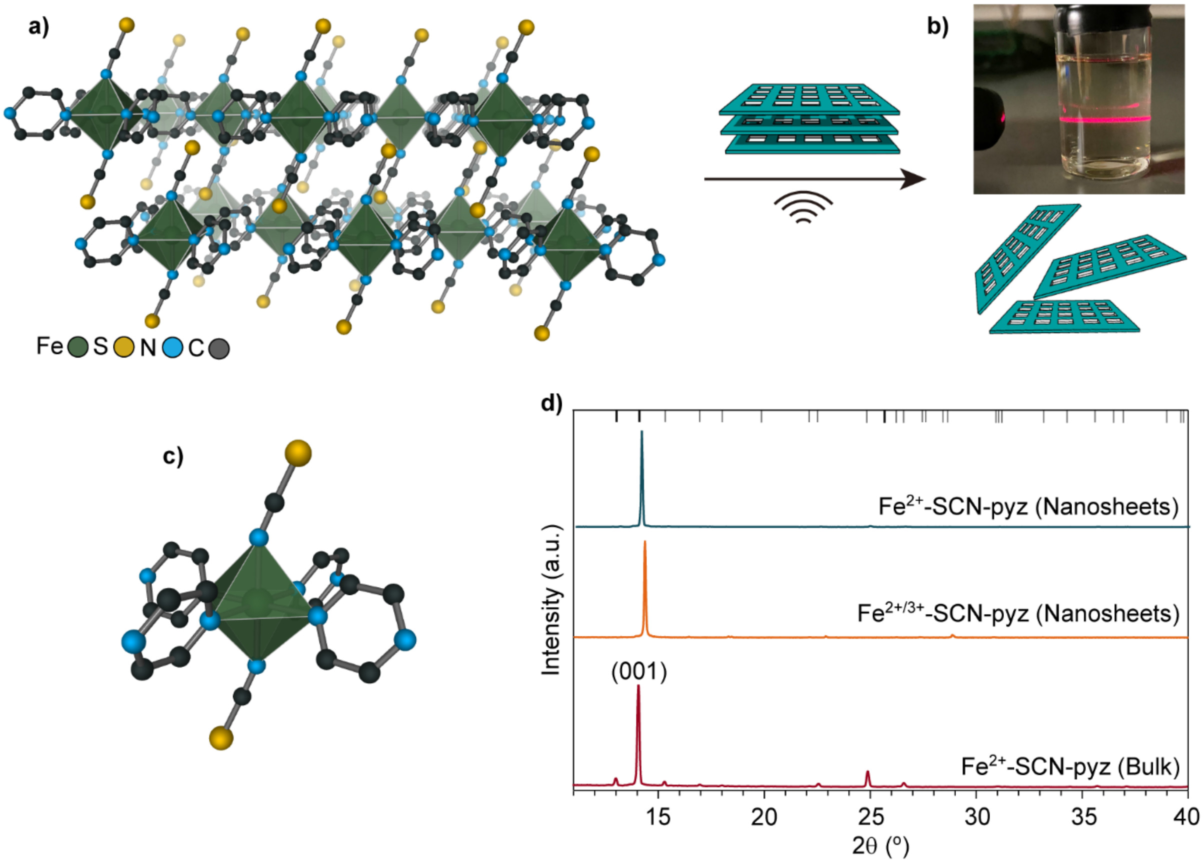

Figure 1: (a) 3D crystalline structure for $Fe(SCN)_2(pyz)_2$. (b) methanolic solution of exfoliated $Fe(SCN)_2(pyz)_2$ displaying the Tyndall effect. (c) local octahedral coordination environment of iron centers. (d) Powder x-ray diffraction patterns for the bulk and exfoliated 2D sheets pre and post atmospheric oxidation

As a powder under aerobic conditions, Fe-SCN-pyz remains bright orange indefinitely, while as a methanolic suspension it progressively darkens from yellow to violet over the course of two weeks. The violet-colored solution still strongly displays the Tyndall effect, however, indicating the sheets remain separated. When dried, this nanosheet suspension yields a dark purple, nearly black powder. The crystallinity of this material is preserved with preferential orientation along the (001) crystallographic plane and a slight shift of the (001) reflection indicating a relative contraction of interlayer spacing in the crystal lattice (**Fig. 1d**). To investigate this stark color change, the samples were measured by solution-state spectroscopy. **Fig. 2a** displays UV-Vis spectra of the materials suspended in MeCN under anerobic conditions and after atmospheric exposure. Both samples show prominent features in the UV region, similar to reported absorption spectrum for the analog material Co-SCN-pyz.[34] Most notably, upon air exposure, a broad and

https://doi.org/10.26434/chemrxiv-2024-n5dl2 **ORCID:** https://orcid.org/0000-0002-8014-7904 Content not peer-reviewed by ChemRxiv. **License:** CC BY-NC-ND 4.0

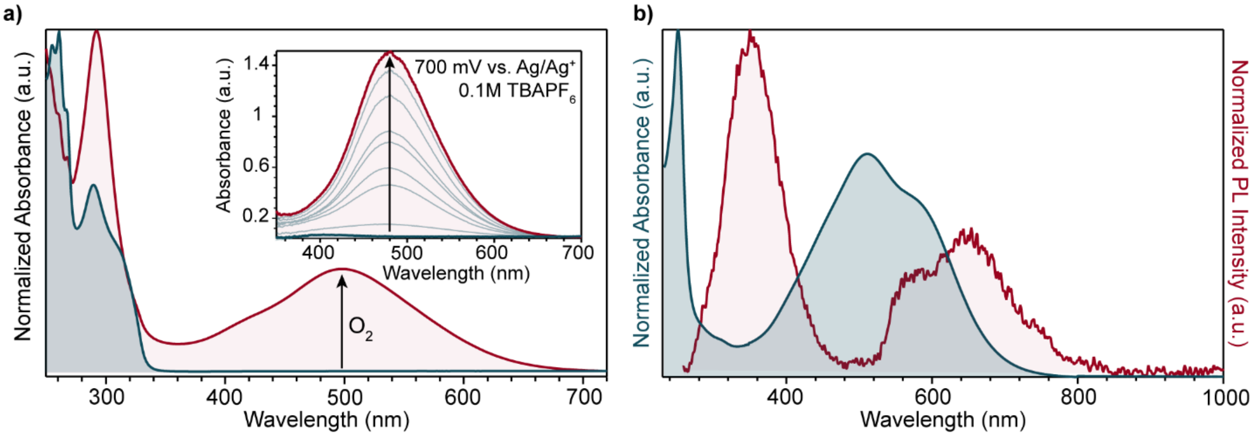

Figure 2: (a) UV-Vis spectrum of exfoliated Fe-SCN-pyz nanosheets suspended in MeCN pre and post atmospheric oxidation. Inset shows UV-Vis spectrum of exfoliated Fe-SCN-pyz nanosheets suspended in a 0.1M TBAPF$_6$ MeCN solution as 700mV vs Ag/Ag$^+$ is applied with a platinum mesh working electrode, platinum wire counter electrode, and silver wire pseudoreference. (b) UV-Vis spectra and photoluminescence spectra of the air oxidized Fe-SCN-pyz nanosheets suspended in DCM after excitation at 250 nm

intense absorption band emerges between 360-700 nm. The intensity and position of the transition suggests the electronic transition is allowed, the breadth suggests it is strongly coupled to vibronic motion, and the energetic position suggests the transition is far below the band gap, all characteristics of intersheet charge transfer excitons.[35–38] Indeed, photoluminescence measurements of the oxidized nanosheets in DCM shows two emission profiles, when exciting at 250 nm **(Fig. 2b)**. The massive red-shift, and low energy emission feature is a hallmark of interlayer excitons. Instead of purely intralayer emission upon excitation, nonradiative electron or hole transfer occurs between layers, generating a charge transfer exciton. Such behavior is common in 2D materials with strong interlayer coupling, but has been limited in study to heterostructure-based films [39–43] Careful observation of the emission and absorption profiles indicates poor spectral overlap between the intralayer excitation and the interlayer absorption, which indicates the nonradiative transfer is a Dexter energy transfer process commonly seen in 2D van der Waal heterostructures.[44,45] The resulting interlayer emission is in close proximity to the assigned interlayer charge transfer in the absorption spectrum, supporting the assignment of this band as a interlayer charge transfer exciton.

To understand the effect of air on the Fe-SCN-pyz oxidation state and the formation of this band, the samples were studied by ^{57}Fe Mössbauer spectroscopy. In contrast to the high-spin Fe^{2+} observed for freshly prepared powder of Fe-SCN-pyz, ^{57}Fe Mössbauer spectra of nanosheets suspended in MeOH and exposed to air for two months exhibit two distinct doublets assignable to high spin Fe^{2+} and high spin Fe^{3+} (**Fig. S12**). Interestingly, even with excessive atmospheric oxidation, the material equilibrates to a mixed valent state with 21% Fe^{2+} and 79% Fe$^{3+.}$ Further evidence of mixed valency was confirmed by diffuse reflectance UV-Vis spectra of air-oxidized

https://doi.org/10.26434/chemrxiv-2024-n5dl2 **ORCID:** https://orcid.org/0000-0002-8014-7904 Content not peer-reviewed by ChemRxiv. **License:** CC BY-NC-ND 4.0

powder, which displayed a broad band in the near IR characteristic of an intervalence charge transfer (IVCT) between Fe^{2+}-Fe^{3+} (**Fig. S6**).

To further understand the interplay between Fe oxidation state and visible light absorption, voltammetric spectroelectrochemistry was performed on a solution of nanosheets suspended in MeCN under anaerobic conditions. The electrochemical cell consisted of a quartz cuvette with a platinum mesh working electrode, platinum wire counter electrode, silver wire pseudo reference lectrode, and 0.1 M $TBAPF_6$ as the supporting electrolyte. Cyclic voltammetry measurements of the suspended nanosheets revealed a reversible redox feature centered at 400 mV vs. Ag that assignable to the $Fe^{2+/3+}$ redox couple (**Fig. S9**). To this solution, a constant 700 mV potential was applied while UV-Vis spectra were recorded in 2-minute intervals. **Figure 2b** displays the growth of an absorption feature at ~500 nm during application of the oxidizing potential. The reversibility of this ~500 nm feature was explored by applying a subsequent 100 mV reducing potential after oxidation, causing the feature to fully bleach. Finally, 700 mV was applied once more and the ~500 nm feature returned (**Fig. S10**).

To identify the underlying mechanism driving optical absorption in solutions of oxidized nanosheets, a series of DFT calculations were performed on monolayer and bulk systems to model the behavior of the material with and without interlayer interactions. First, we obtain the interlayer coupling strength, defined as the energy needed to separate the layered material into individual sheets an infinite distance apart, as a function of Fe oxidation. The fully reduced Fe^{2+} bulk material yields an interlayer binding energy of 2 meV, which is far weaker than the known vdW materials and supports the experimental finding that sonication readily exfoliates the solid material to yield a suspension of monolayer nanosheets. However, when the bulk model system is oxidized to 50% Fe^{3+}, the interlayer spacing contracts by 0.8 Å which is accommodated by axial SCN^- of one layer intercalating within the open square pores of the next layer formed by the pyrazine units. In this contracted, oxidized structure, which is supported by the experimentally observed shift of the (001) PXRD reflection upon aerobic storage, the interlayer coupling energy increases to 64 meV/$Å^2$. This is among the largest interlayer coupling strengths ever reported, and is nearly double the calculated coupling energy of black phosphorous.[46] Furthermore, this demonstrates for the first time the utility of redox in modulating the coupling strength for a material of fixed composition. Additionally, this result suggests that monolayer nanosheets are likely to experience a strong energetic push to aggregate in solution to some extent when oxidation occurs, as the sheets are significantly stabilized by interlayer interactions in the mixed-valent state.

Using both the fully reduced and the mixed-valent models, the optical properties as both monolayers and as bulk systems with interlayer interactions were computed using a model dielectric function to describe the screened Coulomb potential of the excited state. The fully reduced Fe^{2+} material, both as an isolated monolayer and as an aggregated bulk model, features intense absorption between 225 and 350 nm, corresponding to the experimentally assigned pyrazine and SCN^- transitions. In both structural arrangements, any visible absorption is negligible. Similarly, the isolated monolayer of the mixed-valent material only displays significant absorption in the UV range. However, in an aggregated arrangement of the mixed-valent material an intense and broad visible absorption peaking at 510 nm is observed (**Fig. 3a)**. Examination of the wavefunctions associated with the strongest-absorbing excitation reveals an intersheet transition from a donor level centered on the S atom of SCN^- from one layer into the surrounding pyrazine

https://doi.org/10.26434/chemrxiv-2024-n5dl2 **ORCID:** https://orcid.org/0000-0002-8014-7904 Content not peer-reviewed by ChemRxiv. **License:** CC BY-NC-ND 4.0

units which are bonded to the next layer. Because interlayer aggregation is necessary to bring pyrazine into proximity to the interdigitated SCN^-, this transition is only observed in the layered material after oxidation-induced contraction. Indeed, the distance between the S atom of SCN^- and the closest N atom in pyrazine is shortened from 4.09 Å to 3.47 Å in the mixed-valent configuration. These results suggest that upon excitation during fluorescence the excited electron-hole pair is localized pyrazine. While some radiative decay is observed at ~375 nm, given the close 3.47 Å proximity of the pendant SCN^-, the hole can transfer to the SCN^- forming the interlayer exciton that emits at lower energies.

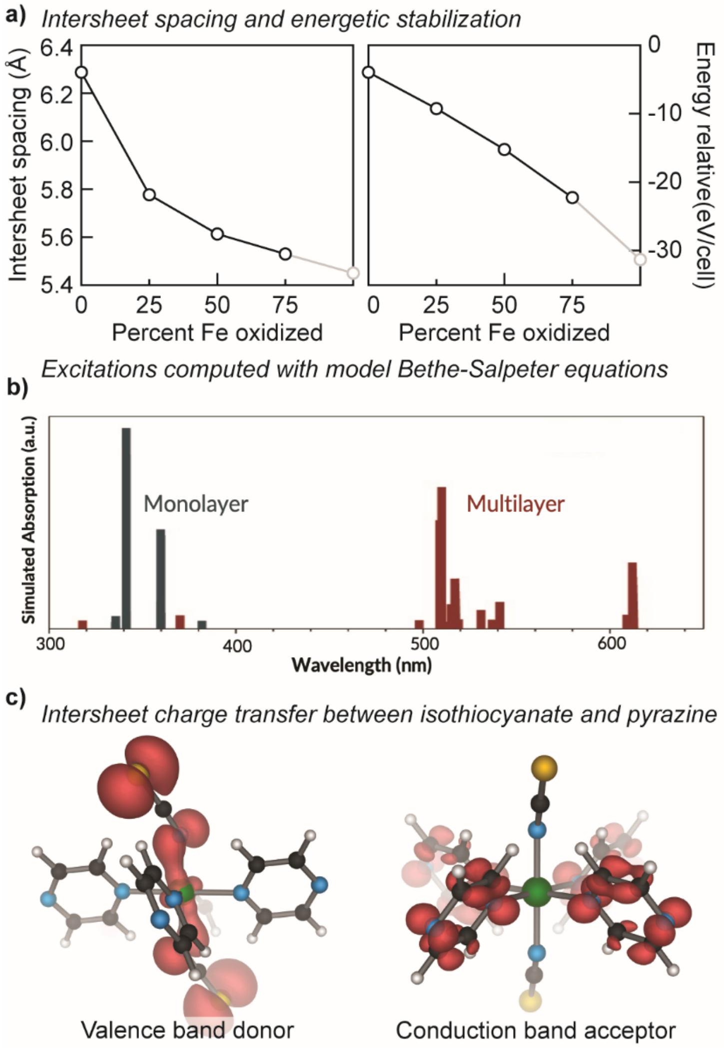

Figure 3: (a) Simulated transitions and relative absorption strength for monolayer and bulk mixed valent 1:1 Fe^{2+}:Fe^{3+}-SCN-pyz. (b) Owing to intersheet exchange interactions, the mixed valent sheets exhibit increased vdW stabilization compared to the fully reduced system. (c) The emergent transition at 510 nm involved transitions between the depicted occupied and virtual bands.

Based on the hypothesis that the broad visible band arises from interlayer charge transfer, and is a charge transfer exciton, we explored the ability of solvent to screen the Coulombic electron-hole interactions. In the UV-Vis response of the isostructural Co-SCN-pyz, authors attribute distinct solvachromatic effects to the dielectric sensitivity of the pendant SCN^- group.[34] With the SCN^- group facilitating interlayer interactions and charge transfer we expected strong

https://doi.org/10.26434/chemrxiv-2024-n5dl2 ORCID: https://orcid.org/0000-0002-8014-7904 Content not peer-reviewed by ChemRxiv. License: CC BY-NC-ND 4.0

solvatochromic effects (**Fig. 4a**).[34] Indeed, in low dielectric solvents (such as Et_2O, THF, and DCM) the interlayer charge transfer band is redshifted, intense, and broad. We interpret this result to mean that weaker solvent-SCN interactions strengthen interlayer interactions, facilitating interlayer charge transfer through increased aggregation and/or increased electron density on SCN. In addition, improved stability of charge transfer excitons by reduced dielectric screening. By contrast, high dielectric solvents blueshift and weaken interlayer charge transfer, with the band nearly unobservable in solvents like MeOH. Strong solvent-SCN interactions weaken interlayer coupling and reduce interlayer charge transfer through weakening interlayer interaction and/or reducing electron density on NCS^-. The high dielectric medium will also facilitate poor exciton lifetime. While it is well known that the dielectric around the exciton has profound effects on its behavior, it has only been explored in 2D heterostructures where insulative layers or organic layers are incorporated between strongly interacting materials to modulate the dielectric response.[47,48] In contrast, due to solution processability and strong interlayer induced aggregation, we report for the first time solvent effects on interlayer charge transfer excitons.

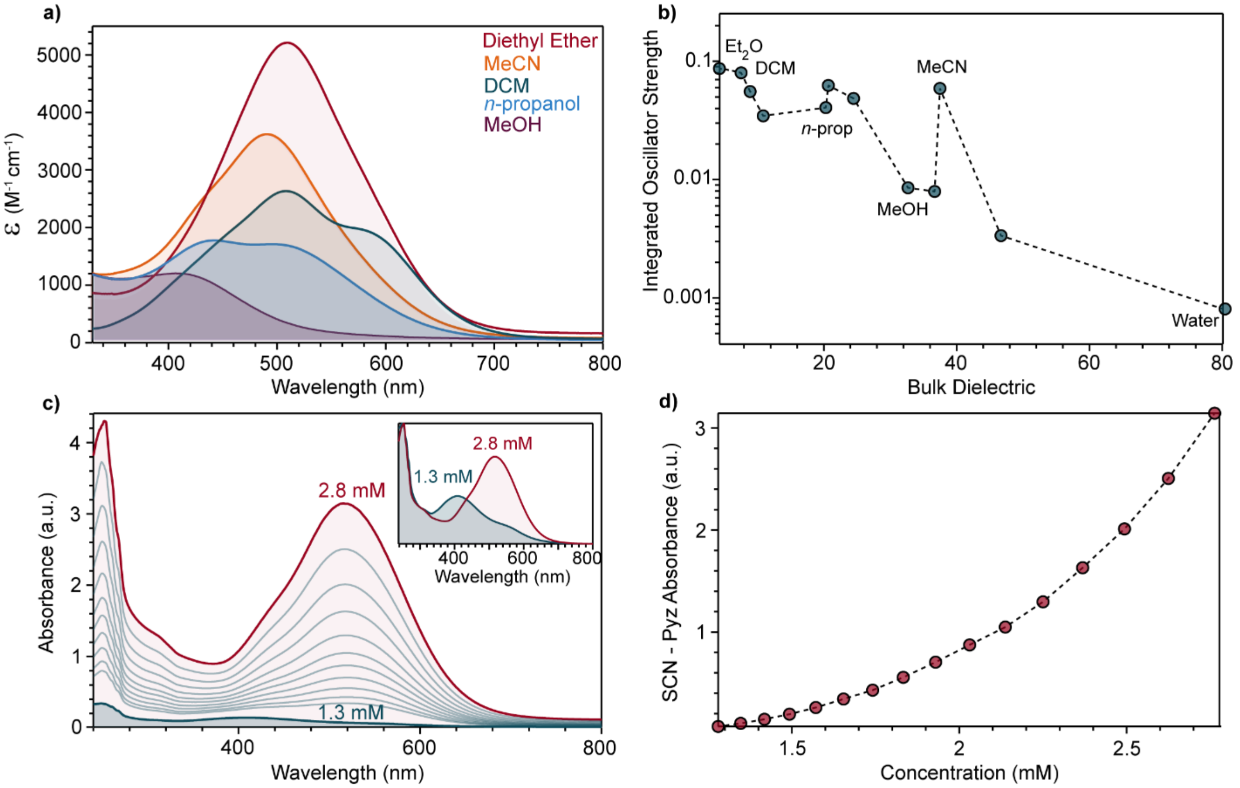

Figure 4: UV-Vis spectrum of atmospherically oxidized Fe-SCN-pyz nanosheets suspended in diethyl ether, MeCN, DCM, *n*-propanol, and MeOH at 184μM (a). Oscillator strength sum across the visible light bands vs solvent dielectric (b) Concentration dependence of atmospherically oxidized Fe-SCN-pyz nanosheets suspended in MeOH (c). Absorption at ~500nm as a function of concentration (d).

Given this evidence that the broadband feature arises from aggregation-induced charge transfer, we explored the effect of interlayer spatial distance. Accordingly, we expected non-linear deviations from Beer-Lambert's law at sufficiently high concentrations where sheets begin to

https://doi.org/10.26434/chemrxiv-2024-n5dl2 **ORCID:** https://orcid.org/0000-0002-8014-7904 Content not peer-reviewed by ChemRxiv. **License:** CC BY-NC-ND 4.0

aggregate.[49] Indeed, suspensions in MeOH at 184 μM in **Figure 4a.** only display a weak band around 400 nm attributed to the $SCN - Fe^{3+}$ charge transfer. For sheets suspended at far higher concentration of 2800 μM, interlayer charge transfer appears (**Fig. 4c**). As shown in Fig. 4d, intensity of the interlayer charge transfer band shows a non-linear concentration dependence at higher concentrations, suggesting aggregation-assisted charge transfer.

As an alternate route to controlling interlayer aggregation, we explored the ability of electrolytes to disrupt these interlayer interactions. Molecular intercalation has been used as a viable method in disrupting interlayer interactions in black phosphorus and in 2D perovskite systems.[50,51] However, they have been limited in scope to strongly interacting molecules which influence electronic structure. **Fig. 5a** shows the UV-vis spectrum of air-oxidized sheets suspended in MeCN with increasing equivalents of inert $TBABF_4$. With greater quantities of electrolyte, the interlayer charge transfer blueshifts and decreases in intensity while features associated with the monolayer Fe-SCN-pyz sheet at ~300 nm increase in intensity. The electrolyte ions stabilize the monolayers in solution and reduce interlayer interactions. As an additional synthetic handle for modulating the size of the intercalating anion, we explored anions of varying size..Adding the larger anion PF_6^- in the form of $TBAPF_6$ to a nanosheet suspension, a comparatively minor

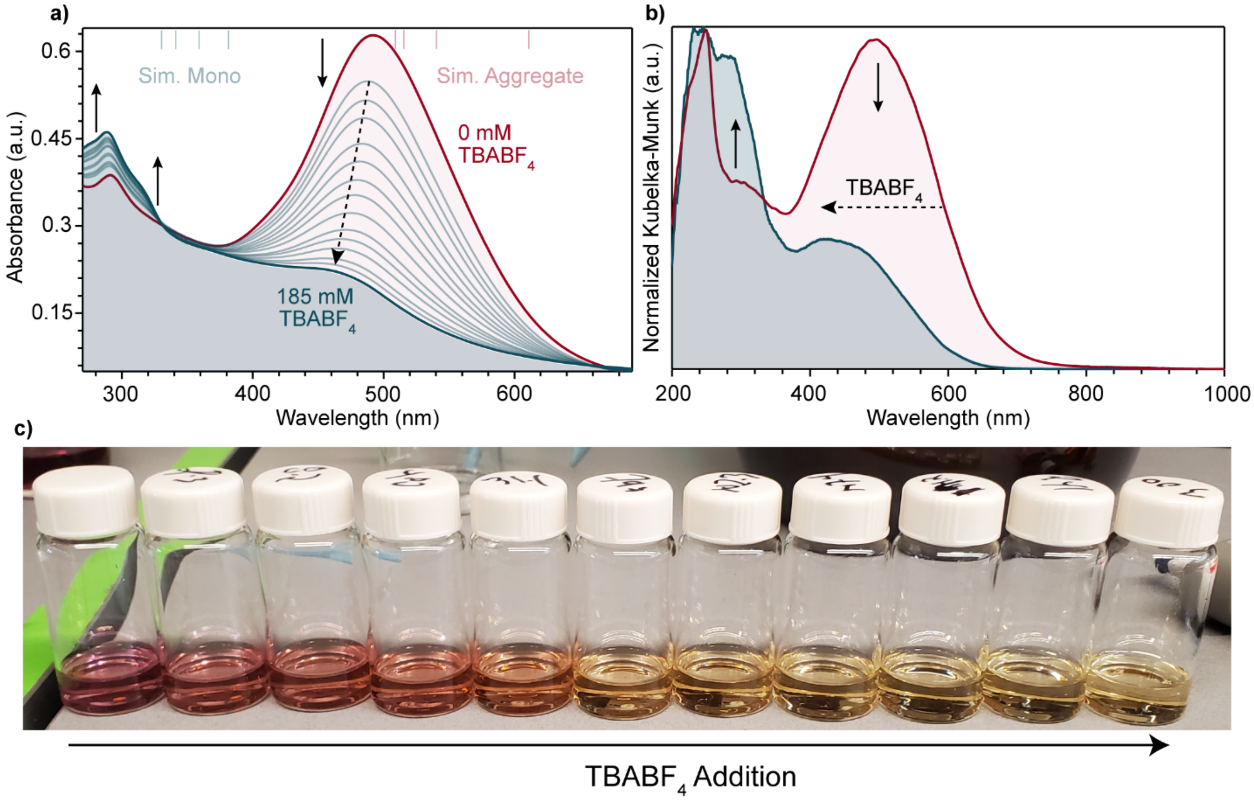

Figure 5: (a) UV-Vis spectrum of atmospherically oxidized Fe-SCN-pyz nanosheets suspended in MeCN as $TBABF_4$ is titrated in (tick marks at top of graph denote the most intense simulated absorptions for mixed valent aggregates and monolayers). (b) DR UV-Vis of atmospherically oxidized Fe-SCN-pyz before and after saturating the pellet with a 1M MeCN solution of $TBABF_4$. (c) Photographic depiction of the solution color change as $TBABF_4$ is added.

https://doi.org/10.26434/chemrxiv-2024-n5dl2 ORCID: https://orcid.org/0000-0002-8014-7904 Content not peer-reviewed by ChemRxiv. License: CC BY-NC-ND 4.0

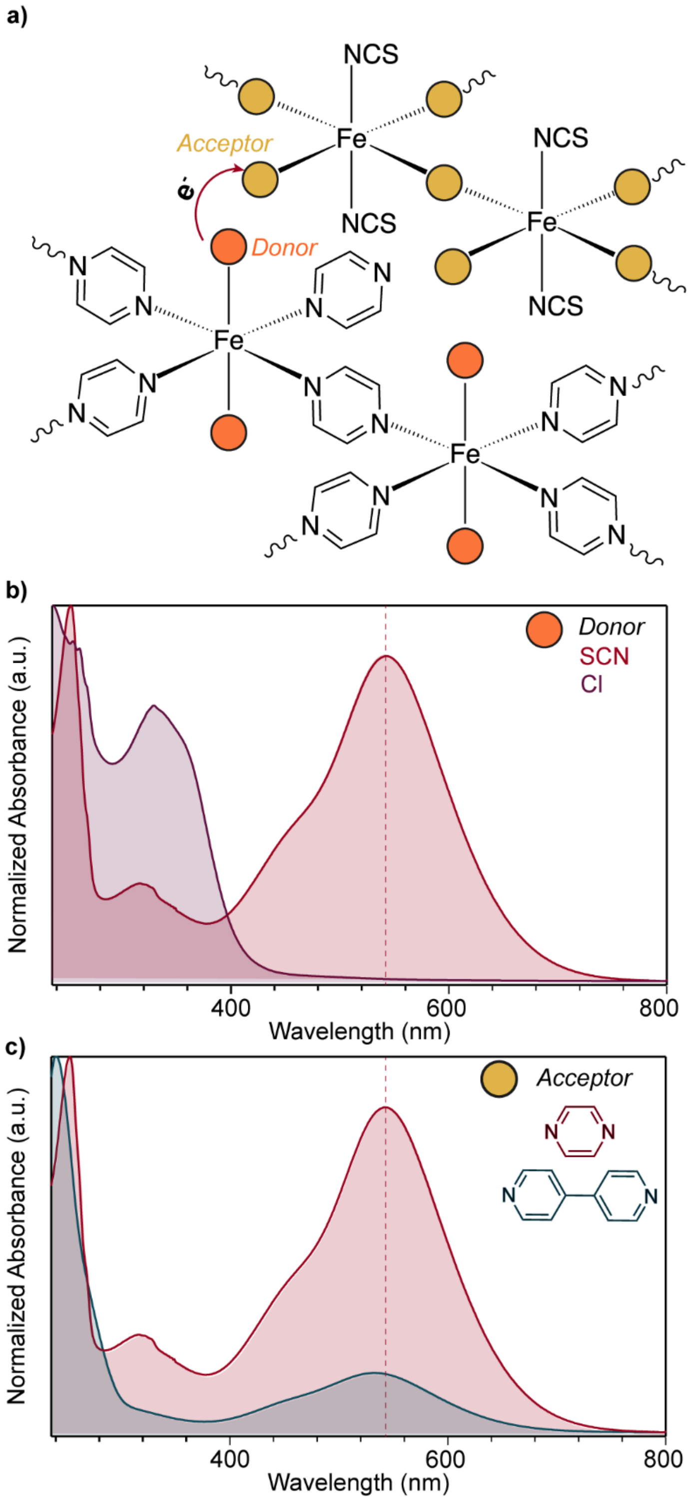

Figure 6: (a) Depiction of the of the donor and acceptor atoms in the interlayer charge transfer. (b) UV-Vis of atmospherically oxidized Fe-SCN-pyz, and Fe-Cl-pyz suspended in THF. (c) UV-Vis of atmospherically oxidized Fe-SCN-pyz and Fe-SCN-4,4'-Bipyridine suspended in THF.

decrease in the interlayer charge transfer band is observed (**Fig. S14**). We interpret this result as

https://doi.org/10.26434/chemrxiv-2024-n5dl2 **ORCID:** https://orcid.org/0000-0002-8014-7904 Content not peer-reviewed by ChemRxiv. **License:** CC BY-NC-ND 4.0

the bulkier PF_6^- proving less effective at intercalating between aggregates and screening charge. Conversely, when the smaller anion NO_3^- from $TBANO_3$ is added to nanosheet suspensions the interlayer band is quenched with addition of relatively few electrolyte equivalents (Fig Sx).

Finally, the synthetic tunability of Fe-SCN-pyz permits microscopic investigation into the structure-function nature of the interlayer charge transfer band. To tune the electronic nature of the donor orbitals, analogous 2D material $Fe(Cl)_2(pyz)_2$ was synthesized. The successful synthesis was confirmed by PXRD (**Fig. S2**). Upon exposure to atmosphere and suspension in THF no visible broadband feature was observed (**Fig. 6c**). However, we do observe a strong band around 360 nm, which we instead assign to a $\mathrm{Cl} - Fe^{3+}$ charge transfer. In a complementary fashion, we tuned the nature of the acceptor orbitals by synthesizing $Fe(SCN)_2(4,4'\text{-bipyridine})_2$ (**Fig. S3**). Unlike Fe-Cl-py and Fe-SeCN-pyz, upon atmospheric oxidation and suspension in THF a purple color was observed. Solution state UV-Vis seen in **Fig. 6b** reveals that the interlayer $\mathrm{NCS} - 4{,}4' -$ bipyridine charge transfer is far weaker and slightly blue shifted relative to the $\mathrm{NCS} -$ pyz charge transfer. We propose that this is due to the strong dependence of the interlayer charge transfer to molecular motion. The ability of 4,4' bipyridine to spin on the bridging methyl axis decreases favorable donor and acceptor orbital overlap, with such molecular dynamics reported in solution.[52]

These results report for the first-time interlayer coupling in 2D MOFs. In summary, Fe^{2+}-SCN-pyz nanosheets in solution exhibit minimal interlayer coupling with a band gap of 3.9 eV, compared to 2.6 eV in bulk. However, with oxidation to $Fe^{2+/3+}$-SCN-pyz there is a strong interlayer stabilizing interaction, shifting the band gap from 3.9 eV to 2.4 eV in THF. This coupling induced by strong SCN^{-}pyz interactions leads to an intersheet exitonic charge transfer. Fe^{2+} oxidation promotes greater interlayer coupling by stabilizing aggregates and reducing distance between SCN^- and pyrazine between layers, even in solution. Solution-state characterization allows for a systematic study into interlayer excitonic absorption. Parameters such as the dielectric medium, concentration, intercalating species, and composition had profound effects on interlayer interactions. Interlayer excitons were observed in solutions of high Fe-SCN-pyz concentrations, low dielectric strength solvents, low electrolyte concentrations, and in materials that contain axial SCN^-.

Conclusion.

In conclusion, we present a combined experimental-computational investigation into interlayer interactions of the van der Waals porous frameworks $Fe(SCN)_2(pyrazine)_2$. Although stable as isolated monolayers when Fe^{2+}, partial oxidation induces strongly bound mixed valent aggregates that generate intense and broad-band interlayer excitons. Due to the inherent tunability of the frameworks, we identified the origin of this charge transfer by systematically altering the composition of the organic and inorganic components. The SCN-to-pyrazine interlayer exciton can be modulated in intensity and peak position by tuning interlayer distance and electronic coupling strengths through changes in solvent, concentration, oxidation state, and electrolyte identity. Taken together, these results demonstrate the ability of molecular orbital interactions to dictate long-range behavior of topological materials.

ACKNOWLEDGMENT.

This material is based upon work supported by the Department of Energy through the Office of Basic Energy Sciences under Grant DE-SC0022147 and by the National Science Foundation

https://doi.org/10.26434/chemrxiv-2024-n5dl2 ORCID: https://orcid.org/0000-0002-8014-7904 Content not peer-reviewed by ChemRxiv. License: CC BY-NC-ND 4.0

through the Division of Materials Research under grant no. DMR-2114430. C.H.H. acknowledges the support from the National Science Foundation under grant no. 2237345 and support from the Camille and Henry Dreyfus Foundation. C.K.B and C.H.H acknowledges the Research Corporation for Science Advancement (Cottrell Award). K.K. acknowledges the Japan Society for the Promotion of Science (JSPS) for an Overseas Research Fellowship (application number 202160772). This work made use of the CAMCOR facility of the Lorry I. Lowkey Laboratories at the University of Oregon.

REFERENCES

(1) Wang, S.; Zhao, S.; Guo, X.; Wang, G. 2D Material-Based Heterostructures for Rechargeable Batteries. *Adv. Energy Mater.* **2022**, *12* (4), 2100864.

(2) Rojaee, R.; Shahbazian-Yassar, R. Two-Dimensional Materials to Address the Lithium Battery Challenges. *ACS Nano* **2020**, *14* (3), 2628–2658.

(3) Li, W.; Liu, C.; Gu, C.; Choi, J.-H.; Wang, S.; Jiang, J. Interlayer Charge Transfer Regulates Single-Atom Catalytic Activity on Electride/Graphene 2D Heterojunctions. *J. Am. Chem. Soc.* **2023**, *145* (8), 4774–4783.

(4) Shen, P.; Yin, P.; Zou, Y.; Li, M.; Zhang, N.; Tan, D.; Zhao, H.; Li, Q.; Yang, R.; Zou, B.; Liu, B. Ultra-Fast Piezocatalysts Enabled By Interfacial Interaction of Reduced Graphene Oxide/MoS_2 Heterostructures. *Adv. Mater.* **2023**, *35* (18), 2212172.

(5) Uri, A.; de la Barrera, S. C.; Randeria, M. T.; Rodan-Legrain, D.; Devakul, T.; Crowley, P. J. D.; Paul, N.; Watanabe, K.; Taniguchi, T.; Lifshitz, R.; Fu, L.; Ashoori, R. C.; Jarillo-Herrero, P. Superconductivity and Strong Interactions in a Tunable Moiré Quasicrystal. *Nature* **2023**, *620* (7975), 762–767.

(6) Niu, R.; Li, J.; Zhen, W.; Xu, F.; Weng, S.; Yue, Z.; Meng, X.; Xia, J.; Hao, N.; Zhang, C. Enhanced Superconductivity and Critical Current Density Due to the Interaction of $InSe_2$ Bonded Layer in $(InSe_2)0.12NbSe_2$. *J. Am. Chem. Soc.* **2024**, *146* (2), 1244–1249.

(7) Wang, H.; Wu, H.; Zhang, J.; Liu, Y.; Chen, D.; Pandey, C.; Yin, J.; Wei, D.; Lei, N.; Shi, S.; Lu, H.; Li, P.; Fert, A.; Wang, K. L.; Nie, T.; Zhao, W. Room Temperature Energy-Efficient Spin-Orbit Torque Switching in Two-Dimensional van Der Waals Fe_3GeTe_2 Induced by Topological Insulators. *Nat. Commun.* **2023**, *14* (1), 5173.

(8) Sauer, M. O.; Taghizadeh, A.; Petralanda, U.; Ovesen, M.; Thygesen, K. S.; Olsen, T.; Cornean, H.; Pedersen, T. G. Shift Current Photovoltaic Efficiency of 2D Materials. *Npj Comput. Mater.* **2023**, *9* (1), 1–9.

(9) Qiao, J.; Kong, X.; Hu, Z.-X.; Yang, F.; Ji, W. High-Mobility Transport Anisotropy and Linear Dichroism in Few-Layer Black Phosphorus. *Nat. Commun.* **2014**, *5* (1), 4475.

(10) Liu, H.; Neal, A. T.; Zhu, Z.; Luo, Z.; Xu, X.; Tománek, D.; Ye, P. D. Phosphorene: An Unexplored 2D Semiconductor with a High Hole Mobility. *ACS Nano* **2014**, *8* (4), 4033–4041.

(11) Qiao, J.; Pan, Y.; Yang, F.; Wang, C.; Chai, Y.; Ji, W. Few-Layer Tellurium: One-Dimensional-like Layered Elementary Semiconductor with Striking Physical Properties. *Sci. Bull.* **2018**, *63* (3), 159–168.

(12) Sutter, P.; Komsa, H. P.; Lu, H.; Gruverman, A.; Sutter, E. Few-Layer Tin Sulfide (SnS): Controlled Synthesis, Thickness Dependent Vibrational Properties, and Ferroelectricity. *Nano Today* **2021**, *37*, 101082.

https://doi.org/10.26434/chemrxiv-2024-n5dl2 **ORCID:** https://orcid.org/0000-0002-8014-7904 Content not peer-reviewed by ChemRxiv. **License:** CC BY-NC-ND 4.0

(13) Zhao, Y.; Qiao, J.; Yu, P.; Hu, Z.; Lin, Z.; Lau, S. P.; Liu, Z.; Ji, W.; Chai, Y. Extraordinarily Strong Interlayer Interaction in 2D Layered PtS_2. *Adv. Mater.* **2016**, *28* (12), 2399–2407.

(14) Sun, Y.; Luo, S.; Zhao, X.-G.; Biswas, K.; Li, S.-L.; Zhang, L. InSe: A Two-Dimensional Material with Strong Interlayer Coupling. *Nanoscale* **2018**, *10* (17), 7991–7998.

(15) Ricci, M.; Ambrosetti, A.; Silvestrelli, P. L. Improving the Description of Interlayer Bonding in TiS_2 by Density Functional Theory. *J. Phys. Chem. C* **2020**, *124* (50), 27592–27603.

(16) Bian, Z.; Miao, J.; Zhao, Y.; Chai, Y. Strong Interlayer Interaction for Engineering Two-Dimensional Materials. *Acc. Mater. Res.* **2022**, *3* (12), 1220–1231.

(17) Dai, Z.; Lu, N.; Liechti, K. M.; Huang, R. Mechanics at the Interfaces of 2D Materials: Challenges and Opportunities. *Curr. Opin. Solid State Mater. Sci.* **2020**, *24* (4), 100837.

(18) Kasai, H.; Tolborg, K.; Sist, M.; Zhang, J.; Hathwar, V. R.; Filsø, M. Ø.; Cenedese, S.; Sugimoto, K.; Overgaard, J.; Nishibori, E.; Iversen, B. B. X-Ray Electron Density Investigation of Chemical Bonding in van Der Waals Materials. *Nat. Mater.* **2018**, *17* (3), 249–252..

(19) Goodman, A. J.; Lien, D.-H.; Ahn, G. H.; Spiegel, L. L.; Amani, M.; Willard, A. P.; Javey, A.; Tisdale, W. A. Substrate-Dependent Exciton Diffusion and Annihilation in Chemically Treated MoS_2 and WS_2. *J. Phys. Chem. C* **2020**, *124* (22), 12175–12184.

(20) Miao, S.; Wang, T.; Huang, X.; Chen, D.; Lian, Z.; Wang, C.; Blei, M.; Taniguchi, T.; Watanabe, K.; Tongay, S.; Wang, Z.; Xiao, D.; Cui, Y.-T.; Shi, S.-F. Strong Interaction between Interlayer Excitons and Correlated Electrons in WSe2/WS2 Moiré Superlattice. *Nat. Commun.* **2021**, *12* (1), 3608.

(21) Qiao, Jingsi, Xianghua Kong, Zhi-Xin Hu, Feng Yang, and Wei Ji. "High-Mobility Transport Anisotropy and Linear Dichroism in Few-Layer Black Phosphorus." *Nature Communications* 5, no. 1. **2014**: 4475.

(22) Duan, F.; Shen, C.; Zhang, H.; Qin, G. Hydrodynamically Enhanced Thermal Transport Due to Strong Interlayer Interactions: A Case Study of Strained Bilayer Graphene. *Phys. Rev. B* **2022**, *105* (12), 125406..

(23) Liu, Y.; Duan, X.; Shin, H.-J.; Park, S.; Huang, Y.; Duan, X. Promises and Prospects of Two-Dimensional Transistors. *Nature* **2021**, *591* (7848), 43–53.

(24) Long, G.; Maryenko, D.; Shen, J.; Xu, S.; Hou, J.; Wu, Z.; Wong, W. K.; Han, T.; Lin, J.; Cai, Y.; Lortz, R.; Wang, N. Achieving Ultrahigh Carrier Mobility in Two-Dimensional Hole Gas of Black Phosphorus. *Nano Lett.* **2016**, *16* (12), 7768–7773.

(25) Viti, L.; Politano, A.; Zhang, K.; Vitiello, M. S. Thermoelectric Terahertz Photodetectors Based on Selenium-Doped Black Phosphorus Flakes. *Nanoscale* **2019**, *11* (4), 1995–2002.

(26) Huang, M.; Wang, M.; Chen, C.; Ma, Z.; Li, X.; Han, J.; Wu, Y. Broadband Black-Phosphorus Photodetectors with High Responsivity. *Adv. Mater.* **2016**, *28* (18), 3481–3485.

(27) Yu, H.; Liu, G.-B.; Tang, J.; Xu, X.; Yao, W. Moiré Excitons: From Programmable Quantum Emitter Arrays to Spin-Orbit–Coupled Artificial Lattices. *Sci. Adv.* **2017**, *3* (11), e1701696.

(28) Mak, K. F.; Shan, J. Opportunities and Challenges of Interlayer Exciton Control and Manipulation. *Nat. Nanotechnol.* **2018**, *13* (11), 974–976.

(29) Lu, Y.; Zhang, Y.; Yang, C.-Y.; Revuelta, S.; Qi, H.; Huang, C.; Jin, W.; Li, Z.; Vega-Mayoral, V.; Liu, Y.; Huang, X.; Pohl, D.; Položij, M.; Zhou, S.; Cánovas, E.; Heine, T.;

https://doi.org/10.26434/chemrxiv-2024-n5dl2 **ORCID:** https://orcid.org/0000-0002-8014-7904 Content not peer-reviewed by ChemRxiv. **License:** CC BY-NC-ND 4.0

Fabiano, S.; Feng, X.; Dong, R. Precise Tuning of Interlayer Electronic Coupling in Layered Conductive Metal-Organic Frameworks. *Nat. Commun.* **2022**, *13* (1), 7240.

(30) Dou, J.-H.; Arguilla, M. Q.; Luo, Y.; Li, J.; Zhang, W.; Sun, L.; Mancuso, J. L.; Yang, L.; Chen, T.; Parent, L. R.; Skorupskii, G.; Libretto, N. J.; Sun, C.; Yang, M. C.; Dip, P. V.; Brignole, E. J.; Miller, J. T.; Kong, J.; Hendon, C. H.; Sun, J.; Dincă, M. Atomically Precise Single-Crystal Structures of Electrically Conducting 2D Metal–Organic Frameworks. *Nat. Mater.* **2021**, *20* (2), 222–228.

(31) Day, R. W.; Bediako, D. K.; Rezaee, M.; Parent, L. R.; Skorupskii, G.; Arguilla, M. Q.; Hendon, C. H.; Stassen, I.; Gianneschi, N. C.; Kim, P.; Dincă, M. Single Crystals of Electrically Conductive Two-Dimensional Metal–Organic Frameworks: Structural and Electrical Transport Properties. *ACS Cent. Sci.* **2019**, *5* (12), 1959–1964.

(32) Pedersen, K. S.; Perlepe, P.; Aubrey, M. L.; Woodruff, D. N.; Reyes-Lillo, S. E.; Reinholdt, A.; Voigt, L.; Li, Z.; Borup, K.; Rouzières, M.; Samohvalov, D.; Wilhelm, F.; Rogalev, A.; Neaton, J. B.; Long, J. R.; Clérac, R. Formation of the Layered Conductive Magnet $CrCl_2(Pyrazine)_2$ through Redox-Active Coordination Chemistry. *Nat. Chem.* **2018**, *10* (10), 1056–1061.

(33) Wriedt, M.; Jeß, I.; Näther, C. Synthesis, Crystal Structure, and Thermal and Magnetic Properties of New Transition Metal–Pyrazine Coordination Polymers. *Eur. J. Inorg. Chem.* **2009**, *2009* (10), 1406–1413.

(34) Luo, Y.-H.; Chen, C.; He, C.; Zhu, Y.-Y.; Hong, D.-L.; He, X.-T.; An, P.-J.; Wu, H.-S.; Sun, B.-W. Single-Layered Two-Dimensional Metal–Organic Framework Nanosheets as an in Situ Visual Test Paper for Solvents. *ACS Appl. Mater. Interfaces* **2018**, *10* (34), 28860–28867.

(35) Mahadevan, S.; Liu, T.; Pratik, S. M.; Li, Y.; Ho, H. Y.; Ouyang, S.; Lu, X.; Yip, H.-L.; Chow, P. C. Y.; Brédas, J.-L.; Coropceanu, V.; So, S. K.; Tsang, S.-W. Assessing Intra- and Inter-Molecular Charge Transfer Excitations in Non-Fullerene Acceptors Using Electroabsorption Spectroscopy. *Nat. Commun.* **2024**, *15* (1), 2393.

(36) Jailaubekov, A. E.; Willard, A. P.; Tritsch, J. R.; Chan, W.-L.; Sai, N.; Gearba, R.; Kaake, L. G.; Williams, K. J.; Leung, K.; Rossky, P. J.; Zhu, X.-Y. Hot Charge-Transfer Excitons Set the Time Limit for Charge Separation at Donor/Acceptor Interfaces in Organic Photovoltaics. *Nat. Mater.* **2013**, *12* (1), 66–73.

(37) Feierabend, M.; Berghäuser, G.; Knorr, A.; Malic, E. Proposal for Dark Exciton Based Chemical Sensors. *Nat. Commun.* **2017**, *8* (1), 14776.

(38) Lukman, S.; Ding, L.; Xu, L.; Tao, Y.; Riis-Jensen, A. C.; Zhang, G.; Wu, Q. Y. S.; Yang, M.; Luo, S.; Hsu, C.; Yao, L.; Liang, G.; Lin, H.; Zhang, Y.-W.; Thygesen, K. S.; Wang, Q. J.; Feng, Y.; Teng, J. High Oscillator Strength Interlayer Excitons in Two-Dimensional Heterostructures for Mid-Infrared Photodetection. *Nat. Nanotechnol.* **2020**, *15* (8), 675–682.

(39) Rivera, P.; Schaibley, J. R.; Jones, A. M.; Ross, J. S.; Wu, S.; Aivazian, G.; Klement, P.; Seyler, K.; Clark, G.; Ghimire, N. J.; Yan, J.; Mandrus, D. G.; Yao, W.; Xu, X. Observation of Long-Lived Interlayer Excitons in Monolayer $MoSe_2$–WSe_2 Heterostructures. *Nat. Commun.* **2015**, *6* (1), 6242.

(40) Aly, M. A.; Shah, M.; Schneider, L. M.; Kang, K.; Koch, M.; Yang, E.-H.; Rahimi-Iman, A. Radiative Pattern of Intralayer and Interlayer Excitons in Two-Dimensional WS_2/WSe_2 Heterostructure. *Sci. Rep.* **2022**, *12* (1), 6939.

https://doi.org/10.26434/chemrxiv-2024-n5dl2 **ORCID:** https://orcid.org/0000-0002-8014-7904 Content not peer-reviewed by ChemRxiv. **License:** CC BY-NC-ND 4.0

(41) Sun, X.; Zhu, Y.; Qin, H.; Liu, B.; Tang, Y.; Lü, T.; Rahman, S.; Yildirim, T.; Lu, Y. Enhanced Interactions of Interlayer Excitons in Free-Standing Heterobilayers. *Nature* **2022**, *610* (7932), 478–484.

(42) Zhu, J.; Shen, F.; Chen, Z.; Liu, F.; Jin, S.; Lei, D.; Xu, J. Deterministic Areal Enhancement of Interlayer Exciton Emission by a Plasmonic Lattice on Mirror. *ACS Nano* **2024**, *18* (21), 13599–13606..

(43) Nagler, P.; Plechinger, G.; Ballottin, M. V.; Mitioglu, A.; Meier, S.; Paradiso, N.; Strunk, C.; Chernikov, A.; Christianen, P. C. M.; Schüller, C.; Korn, T. Interlayer Exciton Dynamics in a Dichalcogenide Monolayer Heterostructure. *2D Mater.* **2017**, *4* (2), 025112.

(44) Liu, J.; Li, Z.; Zhang, X.; Lu, G. Unraveling Energy and Charge Transfer in Type-II van Der Waals Heterostructures. *Npj Comput. Mater.* **2021**, *7* (1), 1–9.

(45) Dong, S.; Beaulieu, S.; Selig, M.; Rosenzweig, P.; Christiansen, D.; Pincelli, T.; Dendzik, M.; Ziegler, J. D.; Maklar, J.; Xian, R. P.; Neef, A.; Mohammed, A.; Schulz, A.; Stadler, M.; Jetter, M.; Michler, P.; Taniguchi, T.; Watanabe, K.; Takagi, H.; Starke, U.; Chernikov, A.; Wolf, M.; Nakamura, H.; Knorr, A.; Rettig, L.; Ernstorfer, R. Observation of Ultrafast Interfacial Meitner-Auger Energy Transfer in a Van Der Waals Heterostructure. *Nat. Commun.* **2023**, *14* (1), 5057.

(46) Huang, Y.; Pan, Y.-H.; Yang, R.; Bao, L.-H.; Meng, L.; Luo, H.-L.; Cai, Y.-Q.; Liu, G.-D.; Zhao, W.-J.; Zhou, Z.; Wu, L.-M.; Zhu, Z.-L.; Huang, M.; Liu, L.-W.; Liu, L.; Cheng, P.; Wu, K.-H.; Tian, S.-B.; Gu, C.-Z.; Shi, Y.-G.; Guo, Y.-F.; Cheng, Z. G.; Hu, J.-P.; Zhao, L.; Yang, G.-H.; Sutter, E.; Sutter, P.; Wang, Y.-L.; Ji, W.; Zhou, X.-J.; Gao, H.-J. Universal Mechanical Exfoliation of Large-Area 2D Crystals. *Nat. Commun.* **2020**, *11* (1), 2453.

(47) Jiang, Y.; Chen, S.; Zheng, W.; Zheng, B.; Pan, A. Interlayer Exciton Formation, Relaxation, and Transport in TMD van Der Waals Heterostructures. *Light Sci. Appl.* **2021**, *10* (1), 72.

(48) Ji, J.; Choi, J. H. Understanding the Effects of Dielectric Property, Separation Distance, and Band Alignment on Interlayer Excitons in 2D Hybrid MoS_2/WSe_2 Heterostructures. *ACS Appl. Electron. Mater.* **2021**, *3* (7), 3052–3059.

(49) Liu, Y.; Liu, H.; Yan, H.; Liu, Y.; Zhang, J.; Shan, W.; Lai, P.; Li, H.; Ren, L.; Li, Z.; Nie, L. Aggregation-Induced Absorption Enhancement for Deep Near-Infrared II Photoacoustic Imaging of Brain Gliomas In Vivo. *Adv. Sci.* **2019**, *6* (8), 1801615.

(50) Wang, C.; He, Q.; Halim, U.; Liu, Y.; Zhu, E.; Lin, Z.; Xiao, H.; Duan, X.; Feng, Z.; Cheng, R.; Weiss, N. O.; Ye, G.; Huang, Y.-C.; Wu, H.; Cheng, H.-C.; Shakir, I.; Liao, L.; Chen, X.; Goddard III, W. A.; Huang, Y.; Duan, X. Monolayer Atomic Crystal Molecular Superlattices. *Nature* **2018**, *555* (7695), 231–236.

(51) Boeije, Y.; Van Gompel, W. T. M.; Zhang, Y.; Ghosh, P.; Zelewski, S. J.; Maufort, A.; Roose, B.; Ooi, Z. Y.; Chowdhury, R.; Devroey, I.; Lenaers, S.; Tew, A.; Dai, L.; Dey, K.; Salway, H.; Friend, R. H.; Sirringhaus, H.; Lutsen, L.; Vanderzande, D.; Rao, A.; Stranks, S. D. Tailoring Interlayer Charge Transfer Dynamics in 2D Perovskites with Electroactive Spacer Molecules. *J. Am. Chem. Soc.* **2023**, *145* (39), 21330–21343.

(52) Kallweit, C.; Haberhauer, G.; Woitschetzki, S. 4,4’-Bipyridine as a Unidirectional Switching Unit for a Molecular Pushing Motor. *Chem. Weinh. Bergstr. Ger.* **2014**, *20* (21), 6358–6365.

https://doi.org/10.26434/chemrxiv-2024-n5dl2 **ORCID:** https://orcid.org/0000-0002-8014-7904 Content not peer-reviewed by ChemRxiv. **License:** CC BY-NC-ND 4.0